Surface Review and Letters, 1950110 (6 pages)

DOI: 10.1142/S0218625X19501105

World Scientific
www.worldscientific.com

FLAME SYNTHESIS OF MoO_3 FILMS AND THEIR FLAME REDUCTION TO MoO_{3-x} FILMS FOR NIR-SHIELDING APPLICATIONS

M. A. HOSSEINI, M. RANJBAR* and A. R. SHAFIEYAN
Department of Physics,
Isfahan University of Technology,
Isfahan 84156-83111, Iran
**ranjbar@cc.iut.ac.ir*

Received 27 May 2018
Revised 13 April 2019
Accepted 1 May 2019
Published 20 June 2019

Recently, defective metal oxides have attracted vast attention for their potential applications arising from their increased free carrier concentration. In this study, monoclinic MoO_3 films have been grown on quartz glass substrates by hydrogen flame synthesis, as a fast and mass-productive method. The MoO_3 films then were reduced to defective MoO_{3-x} by a flame-reduction treatment using a butane torch. After reduction, the localized surface plasmon resonance (LSPR) absorption band appeared in the NIR region that was employed for NIR-shielding applications. Films were reduced at a nozzle-to-sample distance ranging from 1 to 4 cm, and the optical properties of these films were investigated at an optimum distance (2 cm) as a function of reducing duration time ranging from 1 to 20 s. The increase in the inner and outer temperatures were measured in the heat-shielding experiment and the optimum reducing condition was determined. Overall, we have developed a fast, mass-productive and cost-effective method for fabrication of heat-shielding devices based on LSPR effect.

Keywords: MoO_3 film; flame; plasmonic; optical materials and properties; solar energy materials.

1. Introduction

Mo oxide nanostructures are of significant importance for applications such as sensing,[1,2] catalysis,[3,4] energy storage[5] and biological applications.[6] Additionally, the chemical and physical properties of Mo oxide can be tailored by tuning the carrier concentration through reduction of MoO_3.[7–9] Introducing oxygen vacancies, doping of small ions such as Na^+ and H^+ are the most effective ways to control carrier level in the Mo oxide.[9,10] Up to now, several methods have been developed to reduce Mo oxide in order to increase the number of oxygen deficiency and the free carrier concentration. Moreover, treatment of MoO_3 at different temperatures with reducing chemicals is a common reduction method.[11–13] A prolonged process and expensive setup requirements limit the extensive application of these methods.

Alternatively, the flame-reduction method has been proposed to induce oxygen vacancy in a fast and controllable manner in various metal oxides to enhance the photo-electrochemical performance without any significant damage in the morphology and crystallinity.[14,15]

*Corresponding author.

In recent years, the reduced/defective metal oxides have been deeply studied for solar energy harvesting in the NIR region and in the smart-windows applications.[16–22] In order to manipulate the solar energy, the electrochromic (WO_3-based) or thermochromic (VO_2-based) have been developed. They are widely used in smart windows as they can regulate the outdoor vision and heat transfer.[19,20] Moreover, plasmonic metal oxide nanostructures such as tin-doped indium oxide (ITO), Al-doped zinc oxide (AZO) and WO_{3-x} have occupied a prominent place in the infrared shielding applications among the wide variety of selective electromagnetic absorbers.[23–25] Although NIR photothermal conversion properties of plasmonic MoO_{3-x} have been reported,[26] its infrared heat shielding performance has not been paid up to now.

In the present work, we have utilized an all-flame approach to prepare defective MoO_{3-x} films in a cost-effective and mass-productive manner. The obtained MoO_{3-x} exhibited a desirable transparency in the visible region but strong LSPR absorption in NIR, motivating us for investigating their NIR-shielding ability. To our best knowledge, no report exists on flame-synthesized Mo oxide using a solid Mo source for optical applications.

2. Methods

MoO_3 films were prepared by flame-synthesis method using premixed hydrogen and oxygen as the fuel and a Mo plate (2 mm width) as the precursor was inserted at 2 cm from the nozzle into the flame (Fig. 1(a)). A number of quartz glasses ($10 \times 10\,mm^2$) held at room temperature were used as substrates. Oxidation of Mo in the flame provides a streaming down MoO_x vapor, which is deposited onto the quartz substrates. Flame-reduction of prepared MoO_3 films was done using a butane torch (JET.TORCH, PIEZO IGNITION) at various nozzle-to-sample distances for 1 to 20 s. Figure 1(a) shows the schematic of the measured temperatures of the butane flame using a K-type thermocouple. XRD was done by Philips XPERT X-ray diffractometer (CuK_α). Optical spectra were measured by a Perkin Elmer (Lambda 25) spectrophotometer. SEM and TEM were conducted by Hitachi S-4800 and JEOL JEM-2100F, respectively.

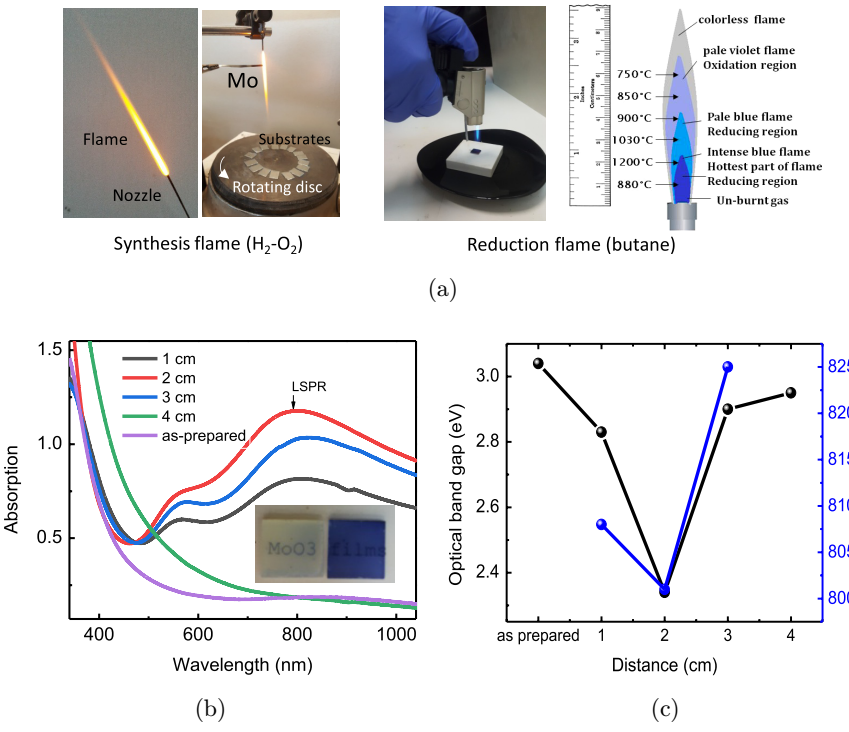

Fig. 1. (Color online) (a) Schematic of hydrogen flame synthesis, flame-reduction and different flame regions, (b) optical absorption spectra of films treated at different nozzle-to-sample distances. Photographic images of as-prepared and reduced (blue) samples. (c) Corresponding optical band gaps and LSPR positions.

To evaluate NIR-shielding performance, a sealed polystyrene box was constructed where Mo oxide coated quartz substrate were used as the window. An IR source (250 mWcm^{-2}) was used to illuminate the box through the window.

3. Result and Discussion

3.1. *Characterization*

The optical absorption spectra of the pristine MoO_3 and flame-reduced films (MoO_{3-x}) are shown in Fig. 1(b). As-prepared and samples reduced at 4 cm have no absorption peak, but LSPR absorption peaks centered at 800–830 nm appear as a result of heat treatment at 1–3 cm nozzle-to-sample distance. The LSPR peak positions and optical band gaps are plotted as a function of nozzle-to-sample distance in Fig. 1(c), indicating reduction treatment at 2 cm provides higher absorption, smaller band gap and shorter LSPR wavelength, while the distance 4 cm acts an oxidizing zone. Appearance of LSPR band at NIR region is related to the formation of oxygen vacancy. The better LSPR properties at 2 cm zone is attributed to its higher temperature and reducing ability, hence 2 cm distance was chosen for the further investigations.

Figure 2(a) shows the XRD patterns of pristine MoO_3 and reduced films at different reducing conditions. The pristine sample could be indexed to monoclinic MoO_3 phase (JCPDS no. 47-1320). In contrast, the XRD pattern of reduced films (MoO_{3-x}) can be broken into patterns of monoclinic MoO_3 and $H_{0.31}MoO_3$ (for 3 and 5 s) or monoclinic MoO_2 (for 20 s). Furthermore, the XRD peak width increases in reduced samples indicating decrease in the crystallite size. Most probably, $H_{0.31}MoO_3$ and MoO_2 both are as intermediate products of reduction of MoO_3 to Mo in flame reduction process. To give more evidence for the importance of the nozzle-to-substrate distance, a typical XRD pattern of a flame-treated sample at

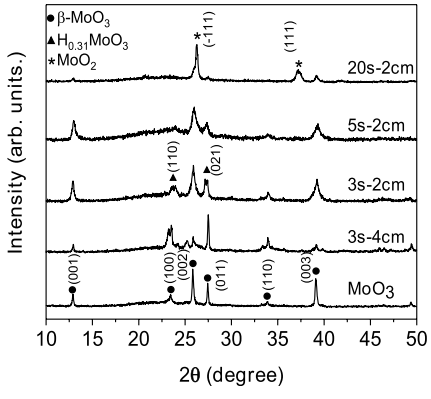

(a)

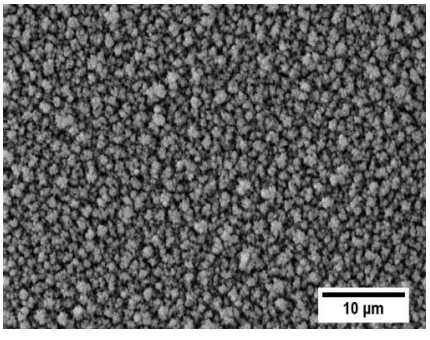

(b)

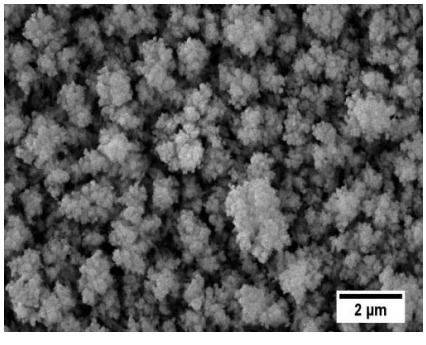

(c)

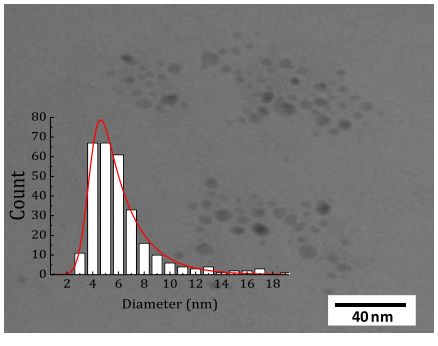

(d)

Fig. 2. (Color online) (a) XRD patterns of films treated at different reducing conditions, (b and c) SEM, TEM images and its size distribution histogram of pristine MoO_3 film.

4 cm for 3 s, is assigned to a well-crystalline monoclinic MoO_3, indicating the oxidizing nature of the flame tip.

The surface morphology of the pristine MoO_3 film is shown in Fig. 2(b). The resulting MoO_3 film represents a homogenous self-assembly of cauliflower-like structures, which at higher magnification image (Fig. 2(c)) are revealed as agglomerates of particles with a nanoscale porosity. The TEM image (Fig. 2(d)) of as-prepared MoO_3 sample, with size distribution histogram, reveals the formation of nanoparticles with dimension 2–20 nm and 5 nm average size.

3.2. *Heat shielding*

In Fig. 3(a), the UV-Vis-NIR transmission spectra of as-prepared and flame-reduced Mo oxide films at distance of 2 cm are shown for 0, 5, 10 and 20 s reducing durations. The pristine sample has about 70% transmission in the visible and NIR region, the rest of which is often scattered from the porous surface. While there is no obvious absorption for the pristine sample, an LSPR absorption band centered at 827 nm appears for 5 s treatment. This is attributed to formation of oxygen vacancy after exposing to reduction zone of the flame. The absorption value of this band reduces and red-shifts when the reduction duration increases to 10 and 20 s. It can be seen that the reduced samples can transmit visible light up to 60% but the absorption edge and the plasmonic band absorb the UV and part of NIR light more than 76%, respectively, which motivate us to investigate their potential for low-cost UV/NIR shielding devices.

It can be seen that sample of 5 s exhibits higher transmittance at visible light but lower at NIR compared with a sample of 10 s. Although sample of 20 s has higher visible transmittance than sample 5 s, it has considerably lower LSPR absorption in NIR light. This is attributed to MoO_2 part of films (see XRD patterns) which is a non-plasmonic phase. Therefore, it is expected that a 5 s reducing duration provides better heat shielding ability.

In order to exploit the shielding properties of flame-reduced films, a heat shielding simulator box was made of window of bare quartz as a reference and MoO_{3-x} coated quartz substrates. Figures 3(b) and 3(c) shows the heat insulation curve of bare quartz and quartz coated with reduced Mo oxide films. Before light illumination, the samples remain at room temperature (21°C). The sun's light radiation on a surface can be reflected, transmitted or absorbed. The absorbed light energy is then transformed into heat via photothermal phenomena. The contact, conduction, and radiation mechanism govern the absorbed heat transmitted inward and outward of the box. Therefore, the analysis of the evolution of temperature inside the box seems to be an ideal method for evaluating the thermal protection capability of reduced MoO_{3-x} films.[26]

Upon light exposure, the inner temperature goes up with increasing time and then represents a slow increase to about 36, 29.5, 31.3 and 31.8°C at 60 min for bare and reduced Mo oxide coated quartz associated with 5, 10 and 20 s, respectively. One can see that the film-covered window associated with 5 s exhibits a slower temperature increasing rate. Figure 3(c) shows the outer (surface of window)

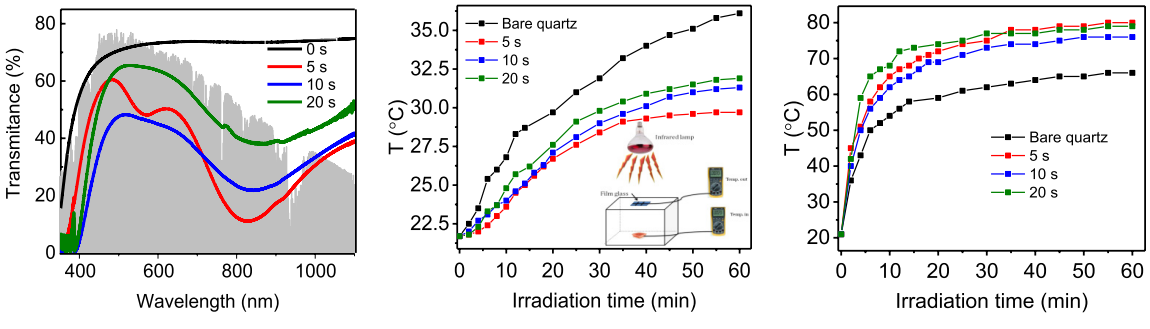

Fig. 3. (Color online) (a) UV-Vis transmission of films reduced at 2 cm for different treatment times, (b, c) inner and outer temperature rise curves in heat-shielding experiment, respectively. For comparison, standard solar spectrum is also plotted.

temperature dependence on irradiation time curves of surface of bare quartz and MoO_3/quartz samples, where an increase followed by a slow increase in temperature is observed for all the sample windows. The heating rate of sample 5 s at window surface is highest and that of blank quartz is lowest among the samples. This effect arises from the photothermal effect of MoO_{3-x} nanoparticles. Therefore, the sample of 5 s treatment exhibits best heating insulating performance in which an inner temperature difference of 8.5°C could be attained attain which is attributed to its better LSPR absorption in NIR region compared to other samples.

In comparison to reduced $CsWO_{3-x}$ nanoparticles with plasmonic peak at ∼1450,[26] our flame-reduced MoO_{3-x} has a plasmonic absorption peak at ∼800 nm. Therefore, a better vision transparency and heat-shielding performance is expected for $CsWO_{3-x}$ films. The thermochromic effects in VO_2 induced a strong NIR absorption but commonly suffer from the less favorable brownish-yellow color and therefore lower visible transmittance of only 30–40% than our flame reduced MoO_{3-x} with 60% transmittance.[27] In addition, toxicity of some vanadium oxides is an important issue in achieving large-scale applications of VO_2.[20] Although the transparent conductive materials such as ITO and AZO have a stronger reflection of NIR light, they can only shield NIR light with a wavelength longer than 1500 nm, which restricted its performance in temperature revolution of simulated house by only 11%, as reported in literature.[28,29] Apart from the device efficiency, the flame synthesis and reduction of MoO_{3-x} introduce a simple, low cost, and mass-productive approach for preparing heat shield windows, which deserves further studies.

4. Conclusion

Based on flame techniques, as a fast and mass-productive synthesis approach, plasmonic Mo oxide films have been prepared on quartz glass for NIR-shielding applications. Hydrogen flame for film growth and butane flame for reduction of grown films were conducted subsequently. For the experimental condition of this work, a sample-to-nozzle distance of 2 cm and a 5 s reducing duration provide an optimum condition for reduction of MoO_3 to defective MoO_{3-x} with a desirable LSPR absorption in NIR region, for which the best heat-shielding characteristic was also achieved. These effects were associated with some structural changes in MoO_3 films as a result of oxygen vacancy formation during the reduction process.

References

1. M. B. Rahmani, S. H. Keshmiri, J. Yu, A. Z. Sadek, L. Al-Mashat, A. Moafi *et al.*, *Sens. Actuators, B Chem.* **145** (2010) 13.
2. K. You, F. Cao, G. Wu, P. Zhao, H. Huang, Z. Wang *et al.*, *Mater. Chem. Phys.* **227** (2019) 111.
3. A. Phuruangrat, S. Thipkonglas, T. Thongtem and S. Thongtem, *Mater. Lett.* **195** (2017) 37.
4. L. Dan, L. Hu, H. Wang and M. Zhu, *Int. J. Hydrog. Energy* (2019).
5. X. Xiao, T. Ding, L. Yuan, Y. Shen, Q. Zhong, X. Zhang *et al.*, *Adv. Energy Mater.* **2** (2012) 1328.
6. T. Bao, W. Yin, X. Zheng, X. Zhang, J. Yu, X. Dong *et al.*, *Biomaterials* **76** (2016) 11.
7. R. Chatten, A. V. Chadwick, A. Rougier and P. J. D. Lindan, *J. Phys. Chem. B* **109** (2005) 3146.
8. T. Ressler, J. Wienold, R. E. Jentoft and T. Neisius, *J. Catal.* **210** (2002) 67.
9. Y. Li, J. Cheng, Y. Liu, P. Liu, W. Cao, T. He *et al.*, *J. Phys. Chem. C* **121** (2017) 5208.
10. H. Cheng, M. Wen, X. Ma, Y. Kuwahara, K. Mori, Y. Dai *et al.*, *J. Am. Chem. Soc.* **138** (2016) 9316.
11. J.-G. Ku, J.-M. Oh, H. Kwon and J.-W. Lim, *Int. J. Hydrog. Energy* **42** (2017) 2139.
12. A. Borgschulte, O. Sambalova, R. Delmelle, S. Jenatsch, R. Hany and F. Nüesch, *Sci. Rep.* **7** (2017) 40761.
13. Q. Zhang, J. N. Lv, X. Y. Hu, Y. L. He, H. F. Yang, D. S. Kong *et al.*, *Int. J. Hydrog. Energy* **43** (2018) 5603.
14. I. S. Cho, M. Logar, C. H. Lee, L. Cai, F. B. Prinz and X. Zheng, *Nano Lett.* **14** (2013) 24.
15. I. S. Cho, J. Choi, K. Zhang, S. J. Kim, M. J. Jeong, L. Cai *et al.*, *Nano Lett.* **15** (2015) 5709.
16. H. Cheng, S. Wei, Y. Ji, J. Zhai, X. Zhang, J. Chen *et al.*, *Compos. A, Appl. Sci. Manuf.* **121** (2019) 139.
17. Q. Gao, X. Wu and L. Cai, *Sol. Energy Mater. Sol. Cells* **196** (2019) 111.
18. M. González, J. Baselga and J. Pozuelo, *Carbon* **147** (2019) 27.
19. C. Guo, S. Yin, Y. Huang, Q. Dong and T. Sato, *Langmuir* **27** (2011) 12172.
20. Y. Cui, Y. Ke, C. Liu, Z. Chen, N. Wang, L. Zhang *et al.*, *Joule*, (2018).
21. S. Ran, J. Liu, F. Shi, C. Fan, B. Chen, H. Zhang *et al.*, *Sol. Energy Mater. Sol. Cells* **174** (2018) 342.
22. C. Yang, J.-F. Chen, X. Zeng, D. Cheng and D. Cao, *Ind. Eng. Chem. Res.* **53** (2014) 17981.
23. J. Xu, Y. Zhang, T.-T. Zhai, Z. Kuang, J. Li, Y. Wang *et al.*, *ACS Nano* **12** (2018) 6895.

24. G. E. Fernandes, D.-J. Lee, J. H. Kim, K.-B. Kim and J. Xu, *J. Mater. Sci.* **48** (2013) 2536.
25. H. Matsui and H. Tabata, *Nanoplasmonics: Fundam. Appl.* (2017) 173.
26. T. Bao, W. Yin, X. Zheng, X. Zhang, J. Yu, X. Dong *et al.*, *Biomaterials* **76** (2016) 11.
27. W. Li, S. Ji, Y. Li, A. Huang, H. Luo and P. Jin, *RSC Adv.* **4** (2014) 13026.
28. H. Matsui, T. Hasebe, N. Hasuike and H. Tabata, *ACS Appl. Nano Mater.* **1** (2018) 1853.
29. A. Sousa-Castillo, Ó. Ameneiro-Prieto, M. Comesaña-Hermo, R. Yu, J. M. Vila-Fungueiriño, M. Pérez-Lorenzo *et al.*, *Nano Energy* **37** (2017) 118.